

COMPARING HF RADAR BACKSCATTER FROM THE SOUTHERN OCEAN WITH RAY-TRACING RESULTS USING THE IRI MODEL

R. J. Norman ⁽¹⁾, M. L. Parkinson ⁽²⁾, and P.L. Dyson ⁽³⁾

⁽¹⁾*Department of Physics, La Trobe University, Victoria 3086, Australia*
r.norman@latrobe.edu.au

⁽²⁾*As (1) above, but E-mail: m.parkinson@latrobe.edu.au*

⁽³⁾*As (1) above, but E-mail: p.dyson@latrobe.edu.au*

ABSTRACT

In this paper, seasonal variations in backscatter from the sea measured with an Over-The-Horizon Radar (OTHR) designed for space weather research are compared to synthesized results generated using advanced numerical ray tracing techniques together with the International Reference Ionosphere (IRI) model. The synthesized results help us to understand changes in the various ionospheric layers causing the features commonly displayed in the real backscatter results. For a given feature, the numerical ray tracing can aid in determining whether it is backscatter from the sea detected via reflections from the E or F layers or sporadic E (Es), or whether it is a result of backscatter from ionospheric irregularities or meteors. Thus the high frequency (HF) radar backscatter, together with the numerical ray tracing technique, offers an important method of remotely sensing the distant ionosphere, and thereby extending our capability to monitor space weather.

INTRODUCTION

In the case of sky-wave propagation, the ionosphere is the medium through which both the transmitted and received signals traverse. A backscattered signal contains useful information regarding the state of the ionosphere at the time and over the propagation path of the returned signal. Methods of synthesising the backscattered signal will provide an important means of remotely sensing the distant ionosphere, as well as remote regions of land and sea. For ground backscatter, the received signals are reflected from distant locations on the Earth's surface, which could be a few thousand kilometers from the transmitter/receiver location. When using steerable high frequency (HF) radar, the ground scatter can be used to infer changes in the ionosphere occurring over millions of square kilometers.

The observed backscatter response depends on the radar system and ionospheric conditions, as well as the backscattering properties of the ground or sea. Important radar characteristics are the transmitter wavelength, pulse length, antenna beam width, antenna gain, and transmitted and received power. If the radar characteristics are known, then changes in the backscatter response due to the ionosphere can be identified. Thus, being able to synthesize the backscattered response can provide a great deal of information regarding space weather, as well as playing an important role in the frequency management of practical Over-The-Horizon Radar (OTHR).

The Tasman International Geospace Environment Radar (TIGER) [1] [<http://www.tiger.latrobe.edu.au/>] is an OTHR which began operations in 1999, and has run almost continuously since then. TIGER looks south from Bruny Island, Tasmania, toward Antarctica, and is designed to study space weather phenomena (e.g., the radio aurora). This basic science instrument will improve our ability to monitor and predict the impact of solar-terrestrial interactions on modern technological systems such as satellite communications, GPS, and OTHR. A second TIGER radar is under construction, and will be deployed near Invercargill, New Zealand. The two radars will make up a dual system with overlapping footprints designed to map ionospheric motions by using crossed radar beams (Fig. 1). TIGER is part of the Super Dual Auroral Radar Network (SuperDARN) [2], [3] which currently consists of 15 radars deployed at high latitudes in both the Northern and Southern Hemispheres. In their standard mode of operation, SuperDARN radars are frequency agile, fix-frequency backscatter sounders.

SuperDARN radars can detect echoes backscattered from 10-m scale magnetic field-aligned irregularities from the ionosphere, as well as backscatter from the Earth's surface. In the case of TIGER, the footprint covers the Southern

Ocean; hence the backscatter observed from the Earth's surface is sea scatter. Since the distribution of sea echoes in the radar footprint depends upon the ionospheric conditions, they can aid in the study of the general properties of the intervening ionosphere, and in modeling ionospheric conditions for users of the HF spectrum.

This paper compares TIGER Tasmania sea-echo observations with numerical ray-tracing results obtained using the International Reference Ionosphere (IRI) [4] to represent the ionosphere. The TIGER observations presented in this paper reveal the diurnal variation in average HF propagation conditions for each season for the year 2000, the first full year of its operation. The ray-tracing results will be compared with the sea-echo observations in the format of group range versus local solar time (LST) plots for a single representative radar beam. The ray-tracing results for ionospheric echoes will be compared in another report.

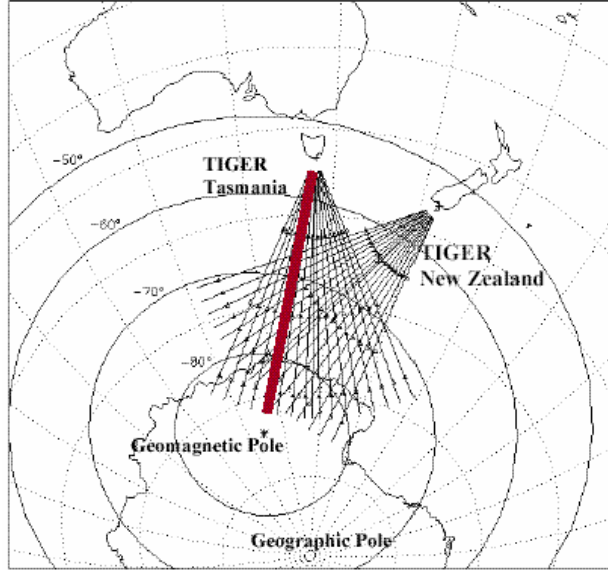


Fig. 1. Field of view of the TIGER radars: TIGER Tasmania (147.2°E , 43.4°S ; 55.0°A) and TIGER NZ (167.7°E , 46.2°S ; 54.5°A). The straight lines represent the 16 azimuthal directions scanned by the $\sim 3^{\circ}$ wide beam of each radar. Beam 4 of the Tasmanian radar (red) points along the geomagnetic meridian. The dotted lines are contours of geographic latitude and longitude, and the solid curved lines are contours of geomagnetic latitude.

SEASONAL OCCURRENCE OF TIGER SEA ECHOES, YEAR 2000

SuperDARN radars employ an array of 16 log-periodic antennas. The use of a phasing matrix enables the main beam to be scanned through 16 pre-defined beam directions (Fig. 1). In this paper, the results for the magnetic meridian pointing beam 4 will be shown because ionospheric structures controlling the HF propagation are approximately L-shell aligned. Our calculations show that beam 4 results are fairly representative of those recorded on other beams.

SuperDARN radars can operate in the frequency range 8–20 MHz, but due to license restrictions, the actual transmission frequencies are usually restricted to a set of licensed bands. To facilitate a meaningful comparison between the observations and ray-tracing results, the occurrence statistics were compiled for echoes recorded in the frequency range $11.0 < f_0 \leq 12.5$ MHz, and the ray-tracing calculations were made at $f_0 = 12.0$ MHz. This frequency corresponds to the maximum radar gain, and not surprisingly, fewer sea echoes were detected at further group ranges and higher operating frequencies (i.e., the normal increase in MUF with group delay).

In the common mode of operation, SuperDARN radars calculate the autocorrelation functions (ACFs) of echoes [1], digitized at 75 range gates starting at 180 km and separated by 45 km (i.e. 180 to 3555 km). The 45-km interval corresponds to the $300\text{-}\mu\text{s}$ width of transmitter pulses. The “FITACF” algorithm [5] processes the ACFs to estimate the echo power in logarithmic units of signal-to-noise ratio (i.e., dB), line-of-sight (LOS) Doppler velocity (m s^{-1}), and the Doppler spectral width (m s^{-1}), for all ranges on every beam. The Doppler characteristics of the echoes are used to determine whether they come from the sea or ionosphere [6]. The current version of FITACF makes use of the LOS

Doppler velocity, v , and the spectral width, w , and their corresponding errors, Δv and Δw , to determine if they come from the sea or ionosphere:

1. Calculate $v - \Delta v$. If the result is less than 0 then set it equal to 0.
2. Calculate $w - \Delta w$. If the result is less than 0 then set it equal to 0.
3. If the result from step 1 is less than 30 m s^{-1} , and the value from step 2 is less than 35 m s^{-1} , then set the ground scatter flag.

The algorithm is vexed because, for example, ionospheric irregularities can also have low velocities and spectral widths, especially for the TIGER radar located at sub-auroral latitudes. Thus sometimes ionospheric echoes will be misinterpreted as sea echoes. The SuperDARN community continues to improve the FITACF algorithm. Nevertheless, the major features to be shown in the observations correspond to genuine sea echoes.

Fig. 2 shows the diurnal variation of TIGER sea-echo occurrence for each season of the year 2000. Results are shown for the four seasons “summer” (a), “winter” (c), “autumn” (b), and “spring” (d). The seasons were redefined to encompass ~90-day intervals centred on the solstices and equinoxes, respectively. Occurrence rates were calculated for all the sea echoes recorded with signal-to-noise ratio $>3 \text{ dB}$ on beam 4, and during quiet to moderate geomagnetic activity ($K_p \leq 3+$). This facilitates comparison of the observations with ray tracing results using the IRI model. Each occurrence rate was calculated by counting the total number of echoes during a 15-min bin of time at each of the 75 ranges, then dividing by the total number of soundings made during that time bin. Thus $96 \times 75 = 7200$ occurrence rates were calculated for each map to reveal the average diurnal variation. The main features shown in each panel are statistically significant. For example, during summer 40,702 beam 4 soundings were made, and 348,066 sea echoes satisfied the selection criteria. The sampling rates were comparable during other seasons [7].

The occurrence rates of sea echoes with signal-to-noise ratio $>3 \text{ dB}$ were shown in preference to average backscatter power because they are more effective at revealing variations in features with low backscatter power, whilst still revealing variations in the features with largest backscatter power. In this respect, they are analogous to a logarithmic plot of backscatter power.

The main features shown in Fig. 2 are the daytime bands of high occurrence rate, mostly $>40\%$ and sometimes $>90\%$. For example, during summer (a), the leading edge of the main feature commences at ~ 05 LST and group range ~ 2500 km, and then by ~ 12 LST descends in group range to ~ 800 km. The leading edge recedes back to great range before disappearing at ~ 21 LST. In contrast, during winter (c), the main feature commences at ~ 07 LST, and the largest occurrence rates, $>60\%$, also finish much earlier at ~ 17 LST. As the ray-tracing results will show, these main features were associated with 1.0-hop E- and F-layer propagation, and were partially controlled by variations in the solar zenith angle.

Secondary features shown in Fig. 2 include the bands of moderate occurrence rate, mostly $<60\%$, confined to the nighttime. For example, during summer (a), this feature commences near 18 LST and is confined between ranges ~ 700 to 1200 km. Beyond midnight, the feature moves to greater range, ~ 800 to 1400 km, and finishes near 5 LST. Similar features occurred during all seasons, and as the ray-tracing results will show, they are consistent with 1.0-hop propagation via nighttime auroral E layers not specified in the IRI model.

The following secondary features are also apparent in Fig. 2, but they will not be directly modeled:

1. There are bands of moderate occurrence (generally $<60\%$) between 00 and 13 LST at group ranges <600 km, and peaking near 06 LST in autumn (b) and spring (d). These echoes are due to 0.5-hop echoes from relatively slow moving meteor trails [10]. They are also apparent in summer and winter, but during summer the occurrence rates in this band are unusually enhanced ($\sim 70\%$) between 07 and 13 LST. This enhancement is caused by 0.5-hop scatter from relatively slow moving sporadic E (Es) irregularities. Mid-latitude-type Es is well known to have its peak occurrence at 10 LST in summer [11]. Our ray-tracing results will show these patchy layers may have been responsible for some of the complicated structures observed in the main features at further ranges.
2. There is a band of high echo occurrence (up to 70%) between 9 and 17 LST and centered on range ~ 500 km during autumn (c). These echoes are vertical incidence, total reflections from the overhead F-region ionosphere. They are received via a weak vertical side lobe, and from near to the F-region cusp of vertical incidence ionosonde traces. The echoes are misinterpreted as sea echoes because the radio waves are approximately orthogonal to the

relatively slow ionospheric motions directly above the radar. They are most prevalent on autumn days when the transmitter frequency is low and f_oF2 is consistently large (the parameter f_oF2 is the plasma frequency corresponding to peak electron density in the F region).

3. There is a horizontal “bite-out” in occurrence rate at range ~ 1215 km, apparent at all times during all seasons, but most clearly defined during autumn (b). This bite out is an artifact caused by bad lags in the ACFs at this group range.

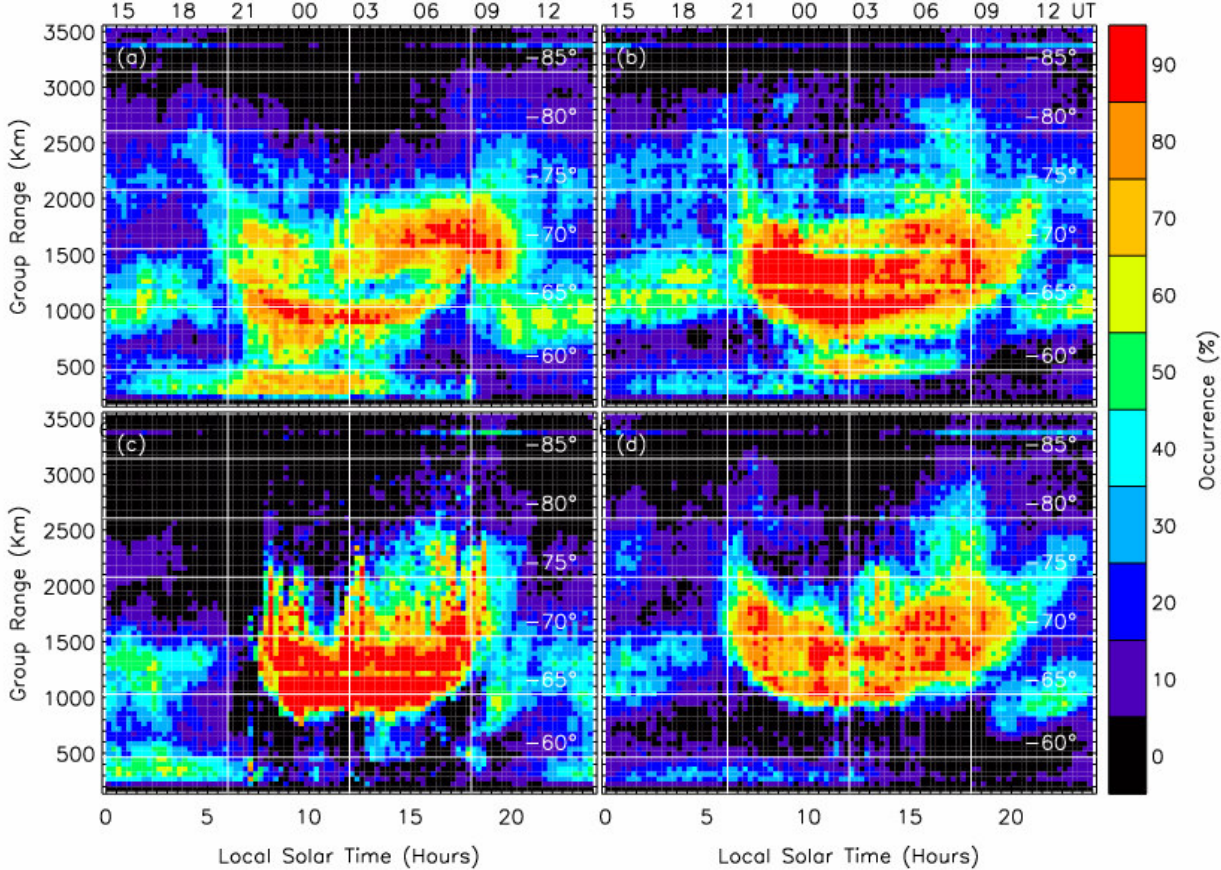


Fig. 2. Occurrence rates of TIGER beam 4 sea echoes for quiet to moderate geomagnetic activity ($K_p \leq 3+$) during (a) summer (days 313 to 035), (b) autumn (days 036 to 126), (c) winter (days 127 to 221), and (d) spring (days 222 to 312) of 2000. The results are shown versus group range and local solar time (LST). Universal time (UT) is shown at top and magnetic latitudes of -60° , -70° , and -80° have been superimposed. These latitudes were calculated using the AAGM co-ordinate system [8] and standard SuperDARN mapping procedures assuming a virtual reflection height of 300 km [9].

SEASONAL VARIATION OF SYNTHESIZED BACKSCATTER POWER, YEAR 2000

Numerical ray-tracing techniques are commonly used for calculating propagation paths taken by electromagnetic waves in a medium, which has an associated refractive index, such as the Earth’s ionosphere. Ray equations derived from Hamilton’s equation are in a form which can be easily integrated numerically by computer. As a result, they are widely used to determine ray paths in the ionosphere. The variational equations necessary to determine a ray tube consisting of the main ray path and two linearly independent variational ray paths was developed ([12] to [15]). Similar techniques were developed independently ([16] to [20]). The method of tracing a ray tube can be used to determine electric field strength and thus backscatter power. The equations given in [15] were restricted to an isotropic medium, so the effects of the Earth’s magnetic field on the ray tube were ignored. The variational ray equations to trace the ray tubes in

anisotropic media, and thus include the effects of the Earth's magnetic field, were re-derived [21]. We use these equations in this study.

The signal strength was determined from the divergence of the ray tube and varies, as does the ray path, with gradients in electron density. Thus an accurate description of the ionosphere is imperative to obtain realistic ray-tracing results. The IRI 2000 model is a widely used empirical ionospheric model [4], and was developed by assimilating data recorded with the worldwide network of ionosondes, as well as incoherent radars, rockets, and satellites. The IRI model provides monthly average values of the ionospheric electron density versus location and height for magnetically quiet conditions. Whilst the IRI model is not designed for high geomagnetic latitudes and disturbance levels, the TIGER radar is located at a geographic mid-latitude (43.4° S), and agreement we obtain proves the applicability of the model to our region.

The synthesized results from the numerical ray tracing will help us to understand the TIGER backscatter results. The ionosphere is made up of a number of distinct layers of increasing electron density. The ray paths that are reflected from each of these layers can be separated, and can then be matched to features in the TIGER results. Two parameters measured by TIGER, namely group path (or time delay) and elevation angle, can be compared directly with the synthesized results. Complete simulations of the backscatter signal strength requires the inclusion of antenna patterns and the magnetic field, and both were included. An Earth centered dipole model was used to represent the Earth's magnetic field. However, the effects due to ionospheric absorption and system losses were not included.

The diurnal variations of sea-echo occurrence shown in Fig. 2 were ultimately caused by average diurnal variations in the ionospheric electron density gradients, as well as the transient perturbations, which did not average away. The electron density gradients in the meridional and vertical direction dominate the refraction of the radio waves, whereas electron density gradients in the transverse direction influence the propagation to a much lesser extent. Fig. 3 shows the IRI model description of the diurnal behavior of f_0F2 for each season of 2000.

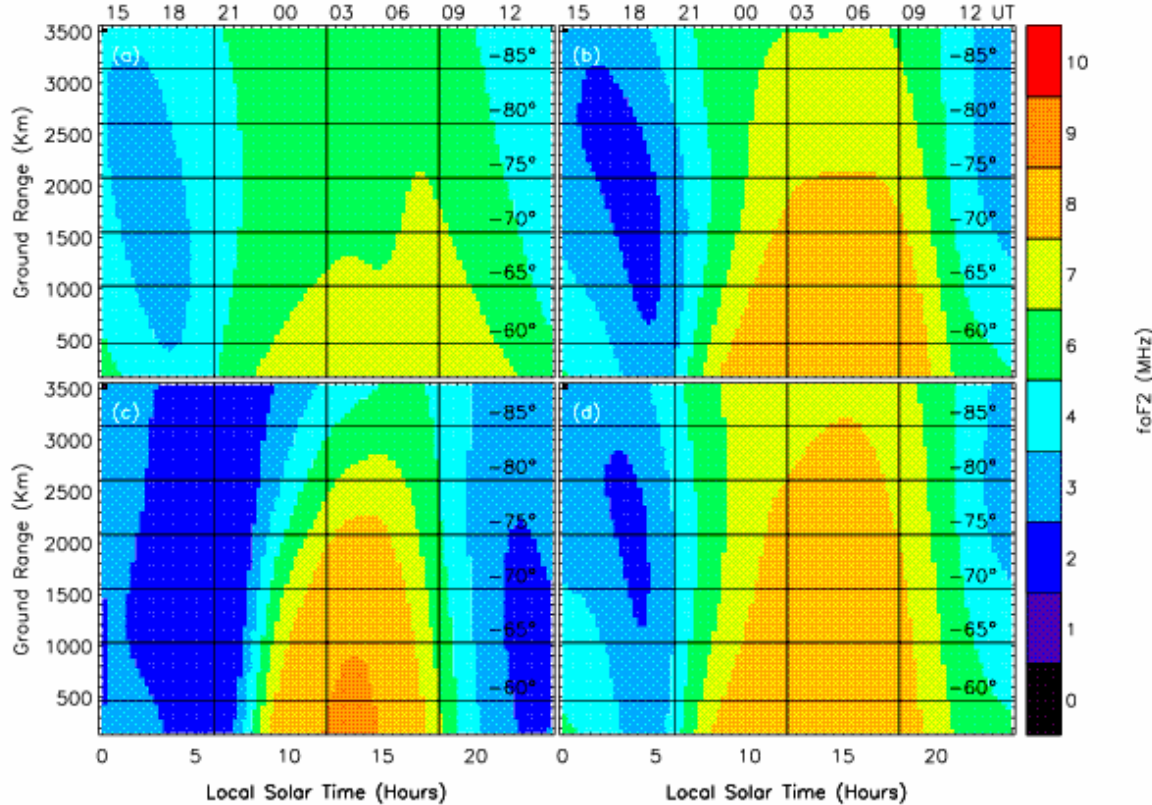


Fig. 3. The IRI model diurnal variations of f_0F2 , from the transmitter location, and in the direction of TIGER beam 4 for each season **(a)** summer (day 356), **(b)** autumn (day 81), **(c)** winter (day 173), and **(d)** spring (day 267).

A value of f_0F2 , in Fig. 3 of say, 6 MHz, means that a vertical incidence ray path requires a frequency greater than 6 MHz to completely break through the ionosphere. The range shown in Fig. 3 represents the true range south along the magnetic meridian, approximately in the direction of TIGER beam 4. The IRI model shows that, in general, there was a strong day-time ionosphere and weak night-time ionosphere, and weakest of all just before sunrise.

Using the numerical ray-tracing program together with the IRI model, the seasonal variation of sea-echo occurrence was synthesised. Fig. 4 shows the diurnal variation of relative backscatter power as a function of group range for each season, using an operating frequency of 12 MHz. The bands of enhanced backscatter power match closely to the corresponding bands of enhanced occurrence shown in the observations, Fig. 2. Note that a dynamic range of 50 dB is shown in Fig. 4, whereas the dynamic range of the radar observations is approximately 40 dB. Hence the weakest features shown in Fig. 4 will not be observed above the noise level in radar observations.

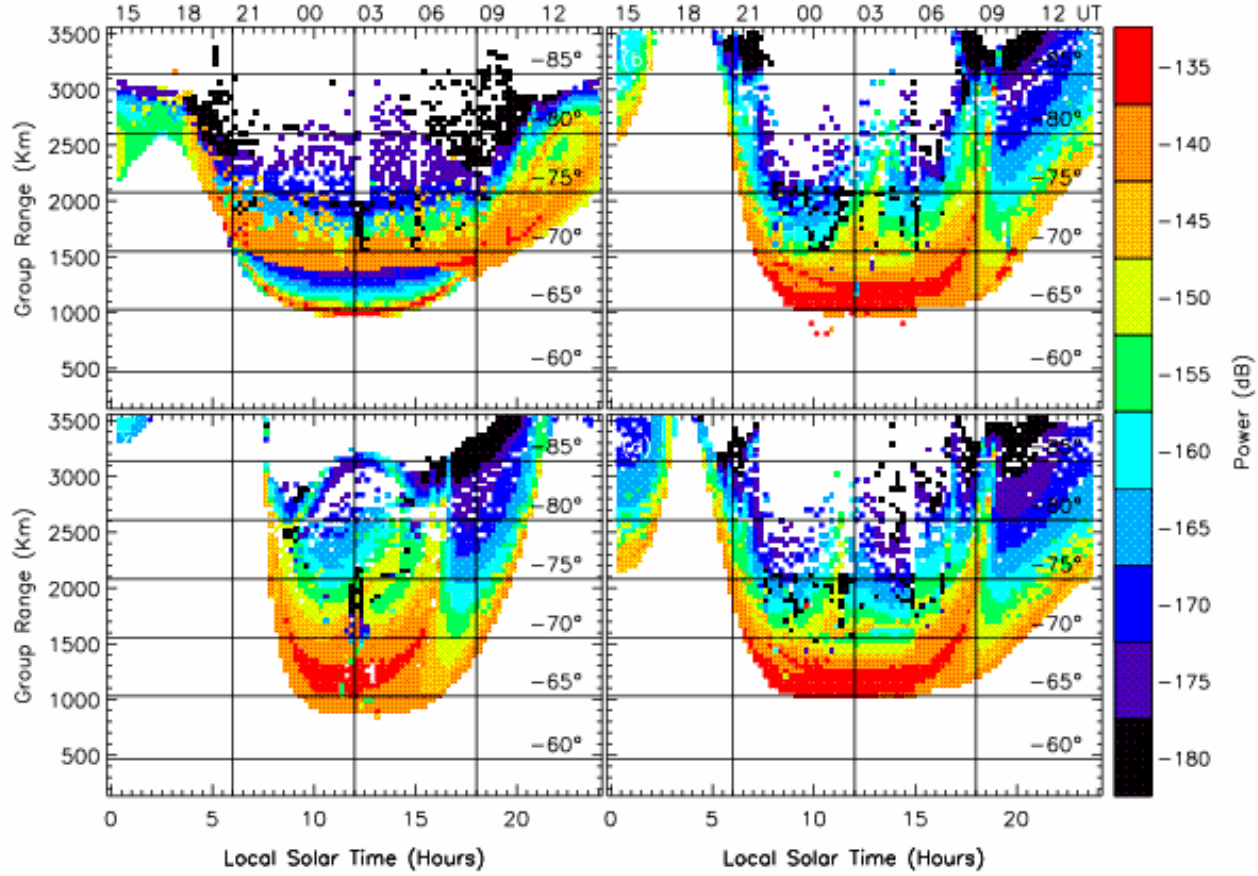


Fig. 4. Seasonal variation of synthesized backscatter power for TIGER beam 4 at $f_0=12$ MHz, and during (a) summer, (b) autumn, (c) winter, and (d) spring of 2000. The powers are on a negative logarithmic scale because they represent divergent power losses relative to the initial transmitted power.

USING SYNTHESIZED RESULTS TO ANALYSE TIGER OBSERVATIONS, YEAR 2000

A greater understanding of variations in TIGER sea echo occurrence can be achieved by comparing them with the numerical ray tracing results. Determining which of the observed features are reflected from the E layer and which are reflected from the F layer is the simplest aspect of the propagation to determine. The effect of other features, such as Es and the main ionospheric trough, can also be identified and then modeled.

(a) Summer Results

The summer observations presented in Fig. 2a were the most complicated, so we concentrate on their analysis and interpretation. There were two distinct day-time propagation modes, represented by the two regions of high occurrence. One region of high occurrence had a group range of ~900 km at ~12 LST, and lasted between ~07 and 17 LST. Another region of high occurrence was displaced ~500 km further away, and lasted between ~06 and 21 LST. These bands of enhanced occurrence are consistent with the corresponding synthesized results shown in Fig. 4a, which show similar bands of enhanced power.

From the synthesized results, it is possible to determine which propagation modes were responsible for each of the two bands. Fig. 5a shows the contribution made by sea-echoes reflected via the E layer, whereas Fig. 5b shows the contribution made by sea-echoes reflected via the F layer. Fig. 5a reveals the corresponding day-time band of large backscatter power in Fig 4a, and the corresponding band of TIGER sea-echo occurrence in Fig. 2a (i.e., group range ~900 km), was associated with E-layer propagation. Similarly, Fig. 5b reveals the corresponding day-time band of large occurrence at group range ~1500 km in Fig. 2a was associated with F-layer propagation.

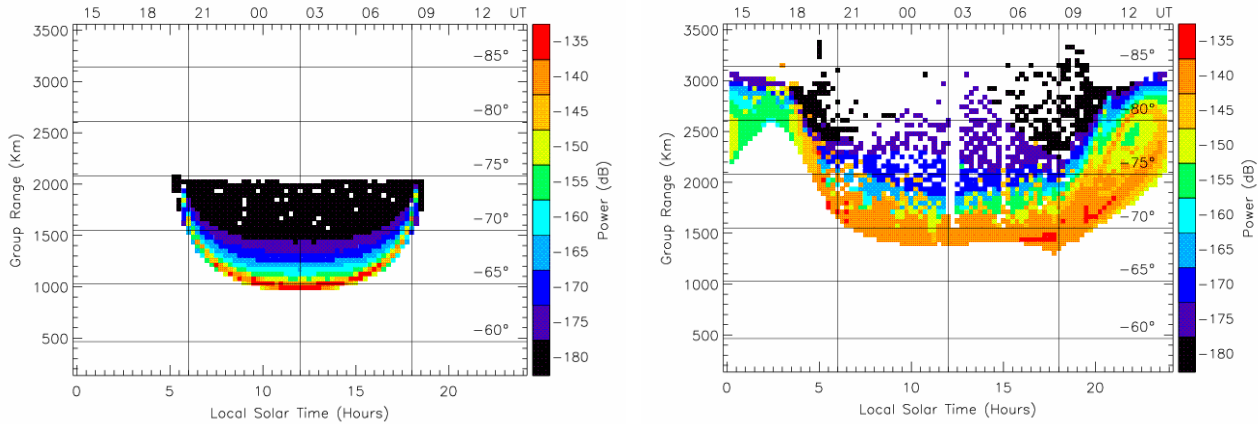


Fig. 5. The same results shown in Fig. 4a, except sorted according to propagation via the **(a)** E layer, and **(b)** F layer.

Fig. 5a reveals that no nighttime sea echoes were propagated via the normal E layer, because this layer was far too weak to reflect the ray paths. Recall an operating frequency of 12 MHz was used for the ray-tracing calculations. However, Fig. 2a showed a secondary sea-echo feature lasted between 18 and 05 LST and had group ranges between ~700 and 1400 km. This feature was caused by genuine 1.0-hop sea echoes, but some of the echoes may have been from relatively slow moving ionospheric irregularities. Hence we conclude the sea echoes were detected by reflection from night-time auroral E layers not included in the IRI model.

In Fig. 2a, another feature lasted between ~07 LT and 11 LT at group range ~700 km. These 1.0-hop sea-echoes were observed via reflection from daytime mid-latitude-type Es, well-known to peak at 10 LST in summer [11]. The presence of these layers partially affected the main F-layer features shown at further group ranges in Fig. 2. Gaps are apparent in the observations, Fig. 2, but not the synthesized results, Fig. 4a. Some of the ray paths that would otherwise reflect from much higher altitudes, and thus have larger group ranges, must have reflected from the lower altitude Es. That is, in a statistical sense, the mid-latitude Es was partially blanketing.

The TIGER radar measures the elevation angle of echoes by calculating the cross correlation function between echoes received on the main and sub-antenna arrays [21]. The numerical ray-tracing program also determines the elevation angle at the transmitter/receiver site. Fig. 6a shows the diurnal variation of elevation angle measured on TIGER beam 4 during summer, and Fig. 6b shows the corresponding ray-tracing results. As expected, in both plots the day-time elevation angles are larger for the ray paths reflected from the F layer than for the ray paths reflected from the E layer. Also, in both cases the elevation angles decrease with group range at the leading edges. Overall, the results for the main features are in reasonable agreement.

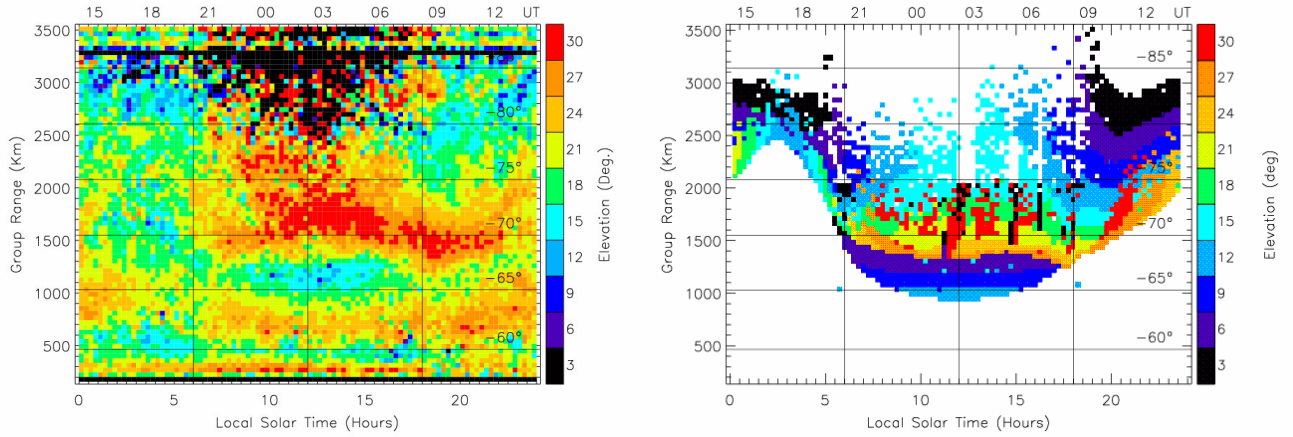


Fig. 6. (a) Average elevation angles measured on TIGER beam 4 during summer, and **(b)** the corresponding ray-tracing results.

(b) Autumn Results

The synthesized results for sea echoes detected during the autumn via normal day time E- and F-layer propagation are shown in Fig. 4b. Again, these are in reasonable agreement with the main feature shown in TIGER observations, Fig. 2b. However, the leading edge for the observations is approximately 250 km closer in group range. We attribute this to variability in ionospheric conditions due to geomagnetic activity, which maximize in autumn [23]. The propagation paths have been shown to shift to lower altitude during energetic particle precipitation [24]. Recall the feature centred on ~ 13 LST at group range ~ 500 km was actually caused by echoes from the overhead ionosphere.

(c) Winter Results

The synthesized results for sea echoes detected during the winter (Fig. 4c) are in good agreement with the corresponding observation (Fig. 2c). Of course, the duration of the main day-time feature is shorter because of the larger solar zenith angles during the winter. The night-time sea-echo features propagated via auroral E persists during all seasons, including winter.

(d) Spring Results

The diurnal variation of sea-echo occurrence during spring was previously modeled [25], and is perhaps the simplest. Here we improve the modeling of spring results by including the effects of propagation via night-time auroral E layers. We have developed techniques to model and map the location of sporadic E patches given the group range of the corresponding ground scatter [26].

In Fig. 7a, the feature located between 00 and ~ 05 LST and group range ~ 700 to 1600 km was caused by reflection from an auroral E layer located 390 km from the radar, and extending a further 410 km toward the south. The feature located between ~ 18 and 24 LST and group range ~ 700 to 1200 km was caused by reflection from an auroral E layer located 360 km from the radar, and extending a further 280 km toward the south. These estimates were obtained using an auroral E layer with peak plasma frequency of 4.0 MHz, peak height 100 km, and half thickness 1 km. Whilst these parameters are somewhat low and thin for auroral E the ray tracing results are relatively insensitive to the choice of parameters, and electric fields and tides will cause the auroral E to converge upon low, thin layers anyway [28]. The gaps in the main F-layer echoes observed and synthesized at greater ranges suggest there are times when the auroral E blanketed propagation to greater heights.

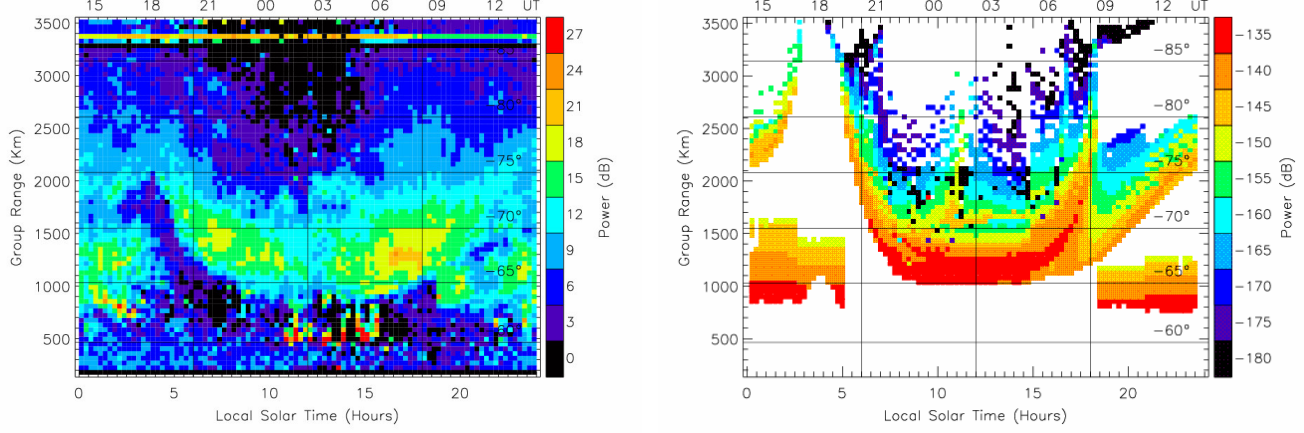


Fig. 7a. (a) Average backscatter power measured on TIGER beam 4 during spring. (b) The corresponding ray-tracing results; the same as Fig. 4d, except the effects of propagation via night-time auroral E layers have been included.

DISCUSSION AND CONCLUSIONS

TIGER, like other SuperDARN radars, was designed to study the ionosphere by measuring the Doppler characteristics of echoes backscattered from ionospheric irregularities. However, ~63% of the echoes detected by the radar are 1.0-hop sea echoes [10], demonstrating TIGER's potential as an OTHR sea-state radar. The results of this paper show the sea echoes can also be modeled using ray-tracing techniques, and thereby used to infer the dynamics of the ionosphere. The diurnal variations of sea-echo occurrence, average backscatter power, and elevation angle measured by TIGER during all seasons of 2000 were in reasonable agreement with the synthesized results obtained by ray-tracing through IRI model ionospheres. This showed the IRI model described ionospheres resembling the seasonal average ionosphere applicable to the TIGER observations. However, there were discrepancies between the ray-tracing results and observations. Recall the radar observations were averaged over all levels of geomagnetic activity during an entire season, whereas the synthesized ray-tracing results used the average quite ionosphere for a single day near the centre of the season. The ray-tracing results also helped us to identify the cause of every other feature shown in Fig. 2, such as those due to meteors, mid-latitude type Es, and night-time auroral E. The success obtained in synthesizing the statistical observations suggest the ray-tracing technique can be adapted to infer real-time ionospheric conditions by inverting and modeling observations recorded on individual days. This is particularly important for HF communications and prediction services where real-time data is required.

ACKNOWLEDGEMENTS

We thank all the engineers and scientists who helped establish, build, maintain, and operate the TIGER radar.

REFERENCES

- [1] P. L. Dyson and J. C. Devlin, "The Tasman International Geospace Environment Radar," *The Physicist* (The Australian Institute of Physics), vol. 37, pp. 48–53, March/April, 2000.
- [2] R. A. Greenwald, K. B. Baker, R. A. Hutchins, and C. Hanuise, "An HF phased-array radar for studying small-scale structure in the high-latitude ionosphere," *Radio Sci.*, vol. 20, pp. 63–79, 1985.
- [3] R. A. Greenwald, et. al., "DARN/SuperDARN: A global view of the dynamics of high-latitude convection," *Space Sci. Rev.*, vol. 71, pp. 761–796, 1995.
- [4] D. Bilitza, "International Reference Ionosphere 2000," *Radio Sci.*, vol. 36, pp. 261–275, 2001.
- [5] K. B. Baker, et. al., "HF radar signatures of the cusp and low-latitude boundary layer," *J. Geophys. Res.*, vol. 100, pp. 7,671–7,695, 1995.

- [6] K. B. Baker, "White paper on FITACF (Update on FITACF for Sept. 2003)," unpublished, September 2003.
- [7] M. L. Parkinson, J. C. Devlin, H. Ye, C. L. Waters, P. L. Dyson, A. M. Breed, and R. J. Morris, "On the occurrence and motion of decametre-scale irregularities in the sub-auroral, auroral, and polar cap ionosphere," *Ann. Geophysicae*, vol. 21, pp. 1,847–1,868, 2003.
- [8] K. B. Baker, and S. Wing, "A new magnetic coordinate system for conjugate studies of high latitudes", *J. Geophys. Res.*, 94, pp. 9,139-9,143, 1989.
- [9] T. K. Yeoman, D. M. Wright, A. J. Stocker and T. B. Jones, "An evaluation of range accuracy in Super Dual Auroral Radar over-the-horizon HF radar systems, *Radio Sci.*, vol. 36, pp. 801-813, 2001.
- [10] G. E. Hall, J. W. MacDougall, D. R. Moorcroft, J.-P. St.-Maurice, A. H. Manson, and C. E. Meek, "Super Dual Auroral Radar Network observations of meteor echoes," *J. Geophys. Res.*, vol. 102, pp. 14,603–14,614, 1997.
- [11] J. D. Whitehead, "Recent work on mid-latitude and equatorial sporadic-E," *J. Atmos. Terr. Phys.*, vol. 51, pp. 401–424, 1989.
- [12] J. A. Bennett, "The applications of variational techniques to radio propagation in the ionosphere," *PhD Thesis*, Melbourne University, 1971.
- [13] J. A. Bennett, "Variations of the ray path and phase path: A Hamiltonian formulation," *Radio Sci.*, vol. 8, p. 737, 1973.
- [14] J. A. Bennett, "Some results for the lateral divergence of ray tubes," *J. Atmos. Terr. Phys.*, vol. 38, p. 529, 1976.
- [15] J. A. Bennett and P. L. Dyson, "New ray tracing techniques and their application to the study of ionospheric irregularities," *Proc. Aust. Inst. Phys. Sixth Nat. Congress*, p. 81, Griffith Uni. Brisbane, 1984.
- [16] C. C. Harvey, "Low frequency waves above the ionosphere," *PhD Thesis*, Cambridge University, 1968.
- [17] R. Buckley, "On the calculation of intensity in dispersive inhomogeneous media in ray approximation," *Proc. Roy. Soc. London, A* 380, p. 201, University Press, 1985.
- [18] K. G. Budden, *The propagation of radio waves*, 1st ed. London, Cambridge University Press, 1985.
- [19] L. J. Nickisch, "Focusing in the stationary phase approximation," *Radio Sci.*, vol. 23, p. 171, 1988.
- [20] A. Vastberg and B. Lundborg, "Signal intensity in the geometrical optics approximation for the magnetized ionosphere," *Radio Sci.*, vol. 31, pp. 1,579–1,588, 1996.
- [21] R. J. Norman, "Ray tracing techniques in anisotropic media," *PhD Thesis*, La Trobe University, 1994.
- [22] S. E. Milan, T. B. Jones, T. R. Robinson, E. C. Thomas, and T. K. Yeoman, "Interferometric evidence for the observation of ground backscatter originating behind the CUTLASS coherent HF radars," *Ann. Geophysicae*, vol. 15, pp. 29–39, 1997.
- [23] C. T. Russel and R. L. McPherron, "Semiannual variation of geomagnetic activity," *J. Geophys. Res.*, vol. 78, pp. 92–108, 1973.
- [24] J. K. Gauld, T. K. Yeoman, J. A. Davies, S. E. Milan, and F. Honary, "SuperDARN radar HF propagation and absorption response to the substorm expansion phase," *Ann. Geophysicae*, vol. 20, pp. 1,631–1,645, 2002.
- [25] P. L. Dyson, R. J. Norman, and M. L. Parkinson, "Ionospheric propagation modes identified using the TIGER HF radar," *Workshop on Applications of Radio Science 2002*, Australian Academy of Science, paper G2, pp. 1–6, 2002.
- [26] R. J. Norman, P. L. Dyson, and J. A. Bennett, "Modelling and mapping sporadic E using backscatter radar," *Australian Solar Terrestrial and Space Physics Research, ANARE Reports 146*, paper 10, pp. 147–164, 2001.
- [27] M. L. Parkinson, J. C. Devlin, H. Ye, C. L. Waters, P. L. Dyson, A. M. Breed, and R. J. Morris, "On the occurrence and motion of decametre-scale irregularities in the sub-auroral, auroral, and polar cap ionosphere," *Ann. Geophysicae*, vol. 21, pp. 1,847–1,868, 2003.
- [28] Parkinson, M. L., P. L. Dyson, D. P. Monselesan, and R. J. Morris: "Formation of sporadic E-layers by magnetospheric electric fields in the southern polar cap ionosphere," *Adv. Space Res.*, 27 (8), pp. 1,399-1,402, 2001.